

Engineering Research Project Report

Training of Activities of Daily Living Using A Rehabilitation Robotic

Mingtian Du mingtiand@student.unimelb.edu.au

Department of Mechanical Engineering, the University of Melbourne

Abstract: *Upper limb disability is common among stroke patients and may impede the activities of daily living. Rehabilitation robotics has been proved to be effective, and experts have developed a rehabilitation robotic named EMU. This kind of robotic requires to be actuated by patients, but severe patients possibly caused by acute stroke do not possess sufficient capabilities to utilize it. This report presents an innovative model to realize automatical and dynamical control to make up the missing function of EMU. The basic idea of the new function is the integration of gradient descent and minimum jerk. Moreover, the model is evaluated by simulation and experiments with five subjects. The model is proved to be feasible for implementation, and the error may be acceptable by preliminary analysis.*

Keywords: *Rehabilitation Robotic, Activities of Daily Living (ADL), Robotic Kinematics, Vision-based Localization.*

1 Introduction

Stroke is the leading cause of disability. Up to approximately 85% of stroke survivors experience hemiparesis (Nichols-Larsen et al., 2005), resulting in an impairment of an upper limb. The functional use of an upper limb extremity is impaired after stroke in approximately 80% of patients acutely and 40% chronically (Nakayama et al., 1994; Parker et al., 1986). Regarding upper limb's functions, the reach-to-grasp is commonly applied to interact with the environment during daily living. However, various motor disorder conditions, such as stroke, are significantly affecting the performance of reach-to-grasp movements (Schaefer et al., 2012). Rehabilitation robots can help disabled patients with diseases related to the nervous system, such as stroke, gain the ability to improve daily life (Choi et al., 2017; Riener et al., 2005). And robotic-assisted intervention for upper-limb rehabilitation has been illustrated to be effective as traditional therapy (Mehrholz et al., 2020).

Ordinary and repetitive movement is crucial while implementing rehabilitation (Nam et al., 2019), so this research focuses on ordinary and high proportion movements - Activity of Daily Living (ADL). Reach-to-grasp movement, an ADL and a purposeful task to accomplish drinking, is associated strongly with activity capacity in participants after stroke (Alt Murphy et al., 2012). Thus, rehabilitation robotics in reach-to-grasp practices is desirable to provide therapy on a specific ADL movement to realize recovery. And although there has been a lot of research and developments on robotics motion, human-like arm motion generations are limited (Gulletta et al., 2020), which shows the necessity of investigating biological solutions.

Engineers from the University of Melbourne collaborated with experts at the Royal Melbourne Hospital, and manufacturer Fourier Intelligence have developed ArmMotus™ EMU shown as Figure 1. This innovative rehabilitation robotic can help patients to practice a large variety of movements by operating on the wrist position (Fong et al., 2017). However, the accomplishment of ADL, such as reach to grasp, require the robotic to be actuated by patients more or less. The acute stroke may result in severe patients who can barely move and do not have sufficient capability to actuate the robotic. Therefore, this project's objective is an automatic and dynamic control to allow this group to proceed with the repetitive practice of ADL. Reach-to-grasp is selected as the case to research because it is general and can be suitable for a large proportion of patients. To achieve this objective, two aspects are currently missing from the EMU system.



Figure 1: Armmotus™ EMU robotic

The dilemma is that people can present redundant movements to reach a target, and each movement may possess a different wrist trajectory and final forearm orientation. These two aspects are relevant to the operation of EMU robotics. Therefore, this report will majorly solve the question of how to design general kinematic computation to imitate biologically natural and human-like reaching movement. This report will present two innovative models to generate a trajectory for the upper limb to solve this dilemma. Simulation and experiments on five subjects are conducted in this report to evaluate the models. Localization systems will be introduced to assist the experiment. Finally, this report indicates one model which requires lower computation and has an acceptable error on wrist trajectory and final forearm orientation. Users' upper limb length will be hypothesized to be known and stable.

2 Literature Review

Some other hypotheses will be indicated in this paragraph. Although the reach-to-grasp movement is familiar, it remains a highly dexterous and sophisticated process. Patients with various degrees of stroke, from mild to moderate to severe, reveal various degrees of predilection about approaching trajectory, grasp orientation, and aperture capability (Schambra et al., 2019). Therefore, this report will hypothesize that a general health human-like movement is desirable for universal patients. Because the age and arm length of the subjects do not significantly affect the wrists' paths while grasping to drink (Wisneski and Johnson, 2007; Murphy et al., 2011), the experiment in this report will not be conducted by requiring subjects from multiple age group and upper limb length group. Collins et al. (2018) apply meta-analysis and conclude that human's reach path ratio (curvature) will differ while placing the object in the central and ipsilateral workspace. So the experiment in this report will be conducted by multiple targets placed central and ipsilateral to evaluate the prospected model's accuracy better.

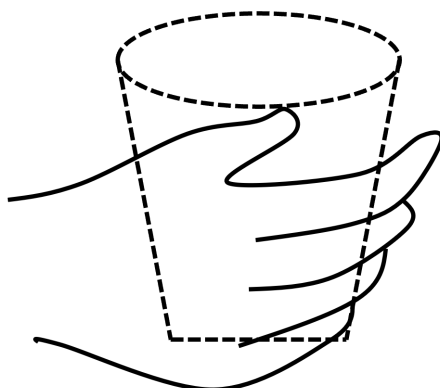


Figure 2: Palmar grasping for cup transportation. The palm and all the fingers wrap around the object and the thumb is in opposition to the other fingers (Garcia Álvarez et al., 2017).

1. The automatic detection and localization of a target object by the robotic system.
2. The dynamical control of a human-like trajectory in achieving a set of ADLs.

The objects' recognition and localization have been well investigated and developed, so it has been guaranteed to be feasible. This research thus concentrates on the second sub-task. Aiming to solve the trajectory problem, this research is expected to design kinematic spatial and temporal trajectory for the reach-to-grasp model by unimanual right-handed movement.

The orientation of the hand when approaching an object depends on many variables, including object shape, size, orientation (Gentilucci et al., 1996), affordance (Wu et al., 2000), location, and properties. This report will assume a regular paper cup as the target to research on reach-to-grasp. And Garcia Álvarez et al. (2017) demonstrate the generally used gesture while grasping for drinking is the Pluri digital and Palmar. The Palmar grasp is commonly used to hold bottles (Popovic et al., 2002) and has been hypothesized in cup transportation experiment (Rounis et al., 2017) manifested in Figure 2. Thus the models in this report will be designed assuming the gesture of Palmar while grasping the target object.

There are various algorithms imposed for computing optimal trajectory, minimum jerk function (Flash and Hogan, 1985) and gradient descent function (Witkin et al., 1987) has been applied to model the reach-to-grasp. And the position trajectory generated by gradient descent and velocity generated by minimum jerk has been verified to be human-like. Based on these two algorithms, three existing models are shown in Table 1. Costa e Silva et al. (2011) computed reach-to-grasp temporal multi-joint angular dynamics for anthropomorphic robotic based on the minimum jerk. This function can only work after knowing the final posture. And Hoff and Arbib (1993) also applied the minimum jerk optimization criterion to formulate a temporal end-point interaction of reach and grasp. However, this function is independent of joint angles, which means there may be a redundancy problem applying inverse kinematics from extreme positions. Torres and Zipser (2002) informed a biological plausible kinematic reach-to-grasp model independent of time. The methodology is cost function and gradient generalizing technique. They use metric transformations to elicit optimized trajectory and develop a more realistic model of the geometric stage by constraint equations. The pros of this function are that it can generate final posture and joint angles only if know the target position. Nevertheless, this function is independent of time, and velocity and acceleration are necessary for dynamical control. Therefore, this report will introduce a new function to generate velocity and acceleration by a minimum jerk on the position trajectory generated by gradient descent.

Equation	Space	Dependency	Approach	Deficiency
Costa e Silva et al. (2011)	Joints Angle	Spatiotemporal	Minimum jerk	Require final posture
Hoff and Arbib (1993)	Extremity State	Spatiotemporal	Minimum Jerk	Independent of joints
Torres and Zipser (2002)	Joints Position	Spatial	Gradient Descent	Independent of time

Table 1: Existing kinematics models classification - ADL for reach-to-grasp. Costa Equation requires final posture, which is unknown. Hoff Equation can only be applied on end-effector without the information of multi-joints. Torres Equation only incorporates the trajectory of positions rather than velocity or acceleration.

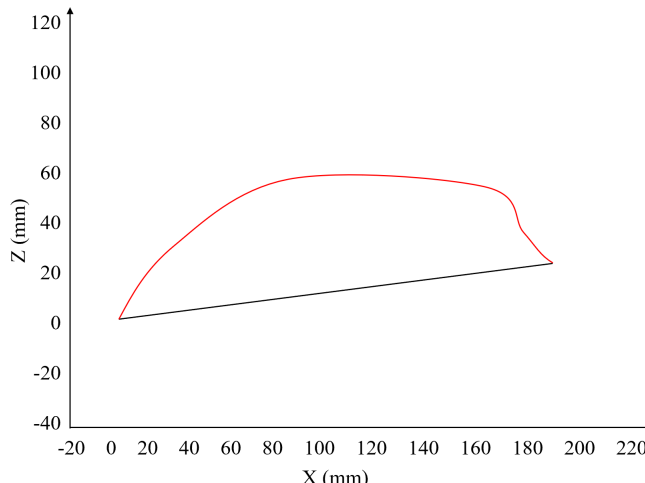


Figure 3: Real trajectory (red) vs. Minimum jerk trajectory (black)

Intuitively defining the final state for reaching and working with minimum jerk may also be feasible because the velocity and acceleration generated by minimum jerk can also derive the position trajectory. However, defining the final state by the final extreme position intuitively can not guarantee that the solution of redundancy is human-like. And defining the general posture by experiment data from five subjects does not possess universality. Besides, Wisneski and Johnson (2007) use experimental data to compare the averaged 3D trajectories and the minimum jerk models to illustrate that the deviation exists among real and ideal trajectories shown as Figure 3. So the positional trajectory will be derived by gradient descent in the function of this report.

3 Methodology

3.1 Kinematics Model

A kinematics model for the general human upper limb is necessary to be designed. Each Degree of Freedom (DoF) is displayed in Figure 4 with each simplified limitation. In the schematic is the initial condition representing that all seven DoFs are equal to zero. DH convention is shown as Table 2.

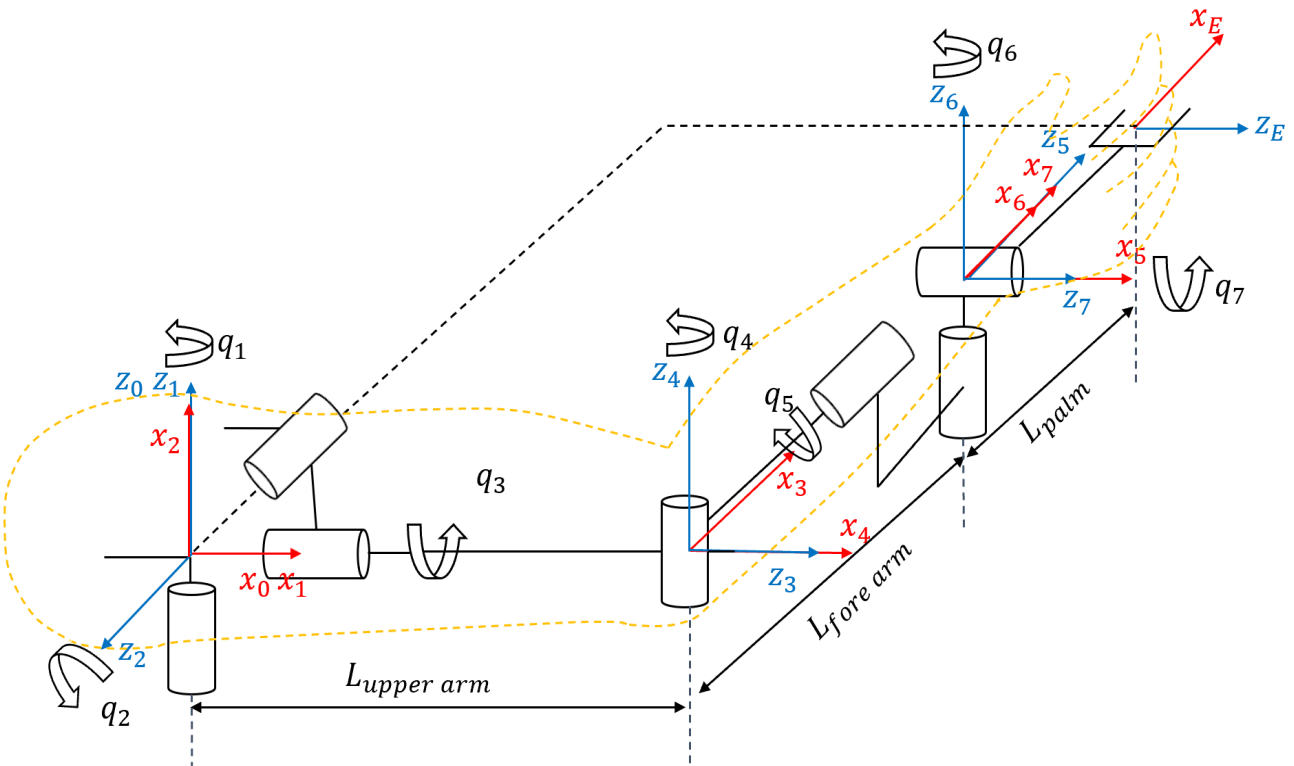


Figure 4: Schematic of human upper limb kinematics model incorporating DoF negative-positive terminology and limitation. q_1 Shoulder Horizontal Extension-Flexion [-90° 90°]. q_2 Shoulder Adduction-Abduction [-90° 90°]. q_3 Shoulder Internal-External [-90° 90°]. q_4 Elbow Extension-Flexion [-90° 90°]. q_5 Elbow Pronation-Supination [-90° 90°]. q_6 Wrist Flexion-Extension [-90° 90°]. q_7 Wrist Radial-Ulnar Deviation [-45° 45°].

i	a_{i-1}	α_{i-1}	d_i	θ_i
1	0	0	0	q_1
2	0	90°	0	$q_2 + 90^\circ$
3	0	90°	L_{up}	$q_3 - 90^\circ$
4	0	-90°	0	$q_4 - 90^\circ$
5	0	-90°	L_{fore}	q_5
6	0	90°	0	$q_6 + 90^\circ$
7	0	90°	0	q_7
E	L_{palm}	0	0	0

Table 2: Denavit-Hartenberg (DH) Convention

After applying the DH convention, the inverse kinematics equations can be derived from the forward kinematics analytically. ${}^0r_{se}$ denotes the vector from shoulder to elbow in frame 0, and ${}^2r_{ew}$ denotes the vector from elbow to wrist in frame 2.

$${}^0r_{se} = [L_{up}\cos(q_1)\cos(q_2) \quad L_{up}\cos(q_1)\sin(q_2) \quad L_{up}\sin(q_1)]^T \quad (1)$$

$$q_1 = \text{atan2}({}^0r_{se_y}, {}^0r_{se_x}) \quad (1)$$

$$q_2 = \text{atan2}({}^0r_{se_z}, {}^0r_{se_x}/\cos(q_1)) \quad (2)$$

After deriving q_1 and q_2 :

$${}^0T = {}^1T {}^1T = \begin{bmatrix} -\cos(q_1)\sin(q_2) & -\cos(q_1)\cos(q_2) & \sin(q_1) & 0 \\ -\sin(q_1)\sin(q_2) & -\cos(q_2)\sin(q_1) & -\cos(q_1) & 0 \\ \cos(q_2) & -\sin(q_2) & 0 & 0 \\ 0 & 0 & 0 & 1 \end{bmatrix}$$

$${}^2r_{ew} = {}_2T^{-1} \times {}^0r_{ew} = [L_{fore}cos(q_4)sin(q_3) \quad L_{fore}sin(q_4) \quad -L_{fore}cos(q_3)cos(q_4)]^T$$

$$q_3 = atan2({}^2r_{ew_x}, -{}^2r_{ew_z}) \quad (3)$$

$$q_4 = atan2({}^2r_{ew_y}, {}^2r_{ew_x}/sin(q_3)) \quad (4)$$

Forward Kinematics will be applied to generate trajectory. Inverse kinematics Equation 1-4 will be applied to calculate initial posture of experimental subjects.

3.2 Trajectory Generation

3.2.1 Distance

Gradient descent is a kind of iterative optimization algorithm to find a local minimum of a differentiable function by repeating steps with step size λ in the opposite direction of gradient Δ . The cost function r should be optimized to be equal to zero or smaller than uncertainty ϵ . And in this model, the cost function represents the distance from the end effector (palm distance from the forward kinematics f_k of joint angles q) to the target x^{target} by the euclidean distance function.

$$r = \sqrt{\sum_{i=1}^3 (x_i^{target} - f_k(q)_i)^2}, \quad q = [q_1 \quad q_2 \quad q_3 \quad q_4 \quad q_5 \quad q_6 \quad q_7]^T \quad (5)$$

$$q = q - \lambda \cdot \Delta r(x^{target}, q), \quad \lambda = diag(\lambda_1, \lambda_2, \dots, \lambda_7) \quad (6)$$

While generating trajectory by gradient descent may require imposing constraints on the function, such as enforcing the joint angles do not surpass the limitation. Torres and Zipser (2002) indicate updated gradient $\tilde{\Delta}$ to impose constraint C .

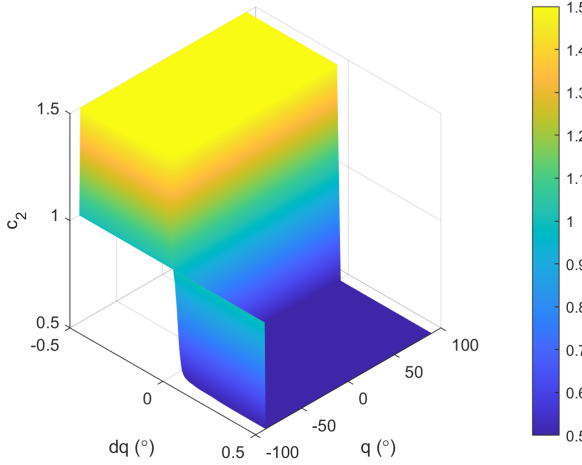
$$\tilde{\Delta}r(x^{target}, q) = C \cdot \Delta r(x^{target}, q), \quad C = diag(c_1, c_2, \dots, c_7) \quad (7)$$

This function can make each joint angle possess different step size value or make the step size be variable while descending. For example, Equation 8, and its surf plot is shown in Figure 5a while assuming the maximum value a^+ is equal to 1.5, the minimum value a^- is 0.5, and the inertial joint angle is q_{rest} . Equation is denoting when joint angle q is away from q_{rest} (differential of joint angle $dq > 0$), c_i is equal to a^- . Conversely, when q is back towards q_{rest} ($dq < 0$), c_i is equal to a^+ . Torres and Zipser (2002) indicate this constraint c_2 can be imposed on q_2 to demonstrate the gravity impact of the upper arm.

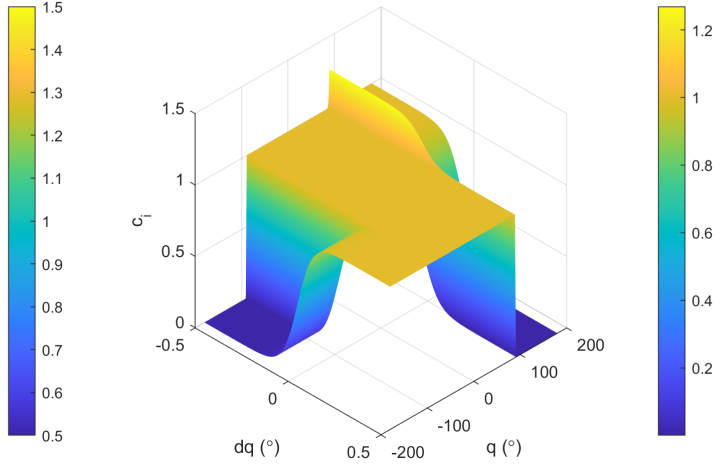
$$c_i = a^+ + \frac{a^- - a^+}{1 + e^{-[(k_1 dq_i)(q_i - q_{rest})]}} \quad (8)$$

Equation 9 can be imposed to realize the limitation of the model, and its surf plot is shown in Figure 5b. When joint angle q is working in its limitation, such as $[q^{min} \quad q^{max}] = [-90^\circ \quad 90^\circ]$, the constraint c_i is equal to one, which means do not impact anything while in original descending. However, when q is surpassing the boundary, which means $q < -90^\circ, dq < 0$ or $q > 90^\circ, dq > 0$, the c_i will be adjusted to be equal to zero to avoid the proceeding variation. And when $q < -90^\circ, dq > 0$ or $q > 90^\circ, dq < 0$, meaning q tends to go back to its workspace, c_i will be kept to be one to allow the returning.

$$c_i = \frac{1}{(1 + e^{[kdq_i]})(1 + e^{[k(q_i^{max} - q_i)]})} + \frac{1}{(1 + e^{-[kdq_i]})(1 + e^{[k(q_i - q_i^{min})]})} + \frac{1}{(1 + e^{-[k(q_i^{max} - q_i)]})(1 + e^{-[k(q_i - q_i^{min})]})} \quad (9)$$



(a) Equation 8 imposing on q_2 with updated step size λa^- to rise up upper arm and λa^+ to low down.



(b) Equation 9 imposing on q_i to avoid it surpassing minimum value q^{min} or maximum value q^{max} .

Figure 5: Surf plot of two constraint equations

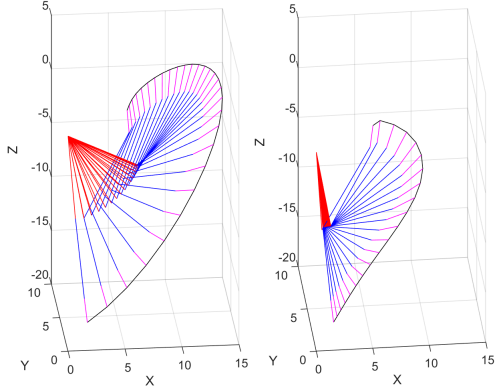


Figure 6: Reproducing of rising up upper limb model.

3.2.2 Distance and Orientation

The cost function r of gradient descent can also incorporate the hand's orientation. Weight value α can be tuned to work with orientation function ϕ . This function is derived from the trace Tr of transformation matrix from extreme to target ${}^t_e T$.

$$r = \sqrt{\sum_{i=1}^N (x_i^{target} - f_k(a)_i)^2 + \alpha(\phi(q, O))^2}, \quad \phi = \arccos\left(\frac{1}{2}Tr[{}^t_e T] - 1\right) \quad (10)$$

Because assumed the Palmar as the standard grasp gesture in this report. Before gathering ${}^t_e T$, fame e need to be rotated from initial e_i to final e_f shown as Figure 7. This rotation aims to guarantee that the hand can grasp the target with the Palmar gesture and that both hand and target orientation are identical. Therefore, transformation from final extreme to target ${}^t_e T$ will replace the transformation from initial extreme to target ${}^t_e T$.

After applying the gradient descent model and imposing two constraint equations on the model, the kinematics trajectory of the upper limb can be demonstrated as Figure 6 independent of the unit. Without constraint equation 8 (left) vs. Imposed. Upper arm (red) - forearm (blue) - palm (magenta) – extreme trajectory (black). This diagram majorly reproduced the variation after imposing Equation 8, from left to right. After imposing this constraint, the upper arm is displayed as relative inert and contributes less than fore arm while rising to reach.

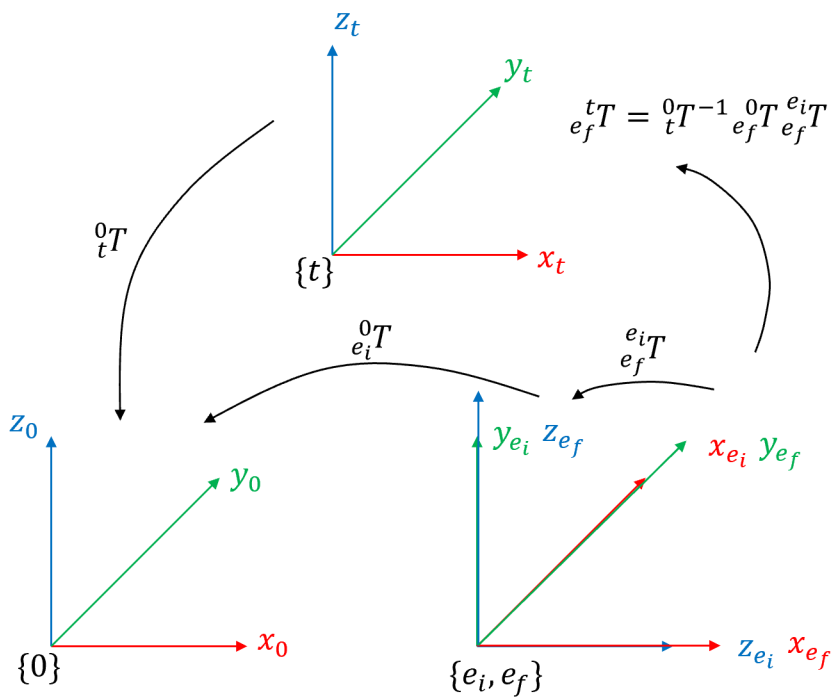


Figure 7: Orientation Schematic about each coordinate system

When extreme possesses the identical orientation to the target, which means:

$$\phi = \arccos\left(\frac{1}{2}\text{Tr}\begin{bmatrix} 1 & 0 & 0 & r_x \\ 0 & 1 & 0 & r_y \\ 0 & 0 & 1 & r_z \\ 0 & 0 & 0 & 1 \end{bmatrix} - 1\right) = \arccos\left(\frac{1}{2} \times 4 - 1\right) = 0$$

However, simply applying this cost function is not reliable in some specific conditions, as shown in Figure 8. Enforcing the hand orientation to be identical to the target may cause abnormal statuses such as dotted schematics in Figure 8a and 8b. In these conditions, solid schematics are intuitively more reasonable instead of dotted schematics where hands have an identical orientation with the target. Therefore, it is necessary to attach a proper coordinate system to the target regarding the particular conditions.

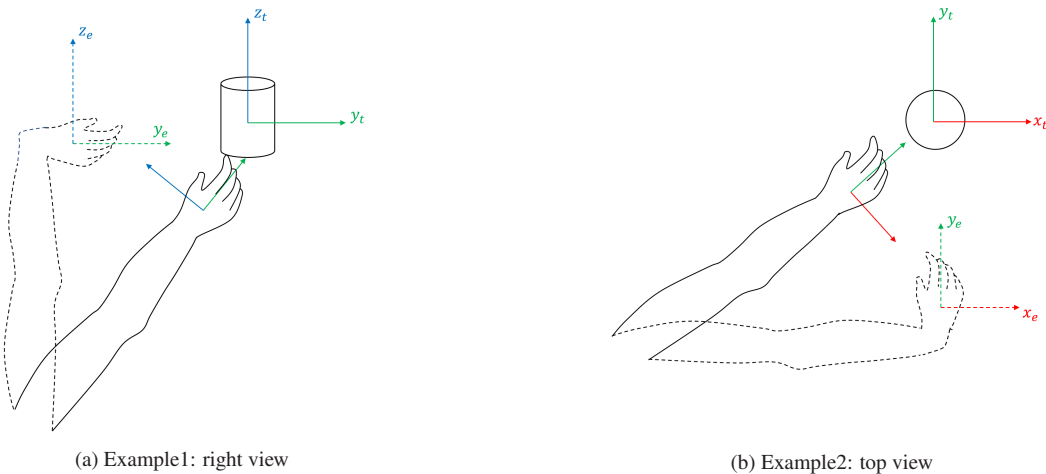


Figure 8: Abnormal conditions if simply applying orientation

One hypothesis proposed in this project is that the hand's final orientation should be relative to the shoulder and target position. Then it is possible to define a hypothetical function for applying the orientation in the cost

function. Attach the updated coordinate frame on the target w.r.t. the shoulder shown as Figure 9a and 9b. The physical meaning is that the final direction of the hand is towards y_{tf} . Besides, there will be rotation along the x and z axes but no rotation along the y axis. The rotation corresponds to only two DoFs of the wrist joint and also corresponds to the assumption that the target is always set on a level platform, z_{ti} , z_{tf} and y_{tf} axes are in a plane.

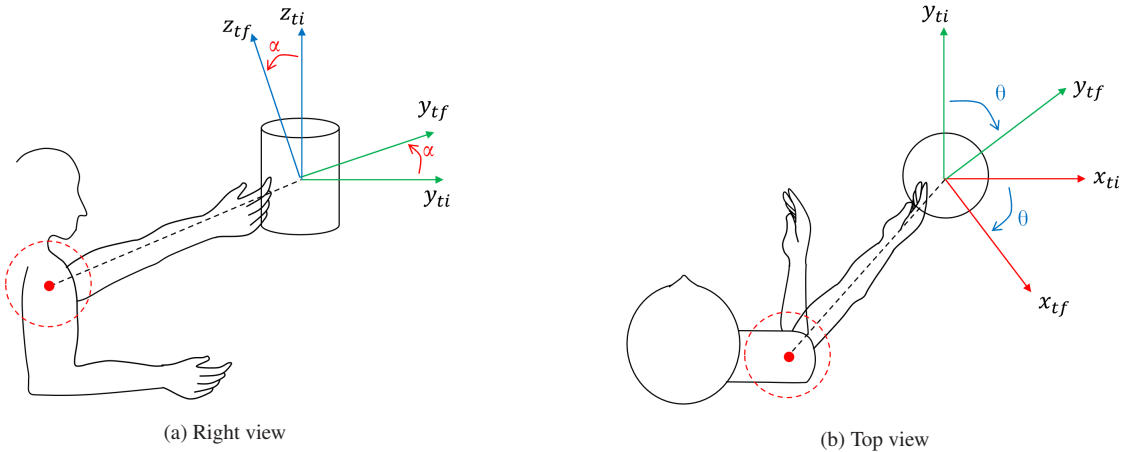


Figure 9: Schematics of how to attach an updated coordinate system on target

$${}_{ti}^f R = R_z(\theta) \times R_x(\alpha) = \begin{bmatrix} \cos(\theta) & -\sin(\theta) & 0 \\ \sin(\theta) & \cos(\theta) & 0 \\ 0 & 0 & 1 \end{bmatrix} \times \begin{bmatrix} 1 & 0 & 0 \\ 0 & \cos(\alpha) & -\sin(\alpha) \\ 0 & \sin(\alpha) & \cos(\alpha) \end{bmatrix}$$

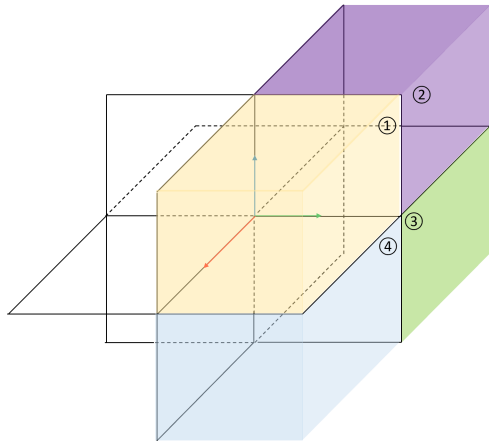


Figure 10: Quadrant schematic. Yellow: quadrant 1. Purple: quadrant 2. Green: quadrant 3. Blue: quadrant 4.

As indicated before, a hypothetical coordinate frame can be attached to the target to define the hand's orientation to grasp the target. If this function is unreliable, we can dispense with using it in the cost function. EMU robotic will manipulate the user's wrist while locking it with a splint. Another pending problem is whether locking the wrist will impact the kinematics in reality and simulation. Therefore, there are four classifications in total, manifested in Table 3. One of four functions is expected to generate reliable human-like kinematic movements. Each performance will be compared by analyzing experiment data.

	Free Orientation	Impose Orientation
Free Wrist	FW-FO	FW-IO
Lock Wrist	LW-FO	LW-IO

Table 3: Four classifications of the existing model. Imposing orientation into the cost function of gradient or not. Locking the wrist or not neglecting the uncertainty may be produced by EMU robotic, whose operating pattern is locking the wrist.

3.3 Addition of Time

Flash and Hogan (1985) indicates that minimum jerk can present a smooth pattern, such as velocity variation, of human arm movement. This technology has been applied for human extremity movement prediction (Hoff and Arbib, 1993) or trajectory interpolation (Costa e Silva et al., 2011). As Wisneski and Johnson (2007) indicates, the real trajectory presents a curved trajectory instead of a straight line generated by a minimum jerk. We have generated a series of waypoints to formulate a trajectory from previous sections. This section is about how to apply minimum jerk to interpolate velocity to each waypoint. The expectation is to elicit a continuous trajectory equation for each segment between each adjacent two waypoints. The continuous equation can be further discretized to be applied to controller modules.

Jerk is the time derivative of acceleration. And to construct a jerk function that has the minimum value, the sixth derivative should be equal to zero, which means a seven polynomial equation for each trajectory shown as Equation 11.

$$x(t) = \begin{cases} p_{10} + p_{11}t + p_{12}t^2 + p_{13}t^3 + p_{14}t^4 + p_{15}t^5 & t_0 \leq t \leq t_1 \\ p_{20} + p_{21}t + p_{22}t^2 + p_{23}t^3 + p_{24}t^4 + p_{25}t^5 & t_1 \leq t \leq t_2 \\ \vdots & \vdots \\ p_{m0} + p_{m1}t + p_{m2}t^2 + p_{m3}t^3 + p_{m4}t^4 + p_{m5}t^5 & t_{m-1} \leq t \leq t_m \end{cases} \quad (11)$$

And jerk equation $j_i(t)$ for each segment is:

$$j_i(t) = x_i^{(3)}(t) = 6p_{i3} + 24p_{i4}t + 60p_{i5}t^2 \quad (12)$$

We can assume vectors \mathbf{a} and \mathbf{p}_i to construct $j_i(t) = \mathbf{a}^T \mathbf{p}_i$:

$$\mathbf{a} = [0 \ 0 \ 0 \ 6 \ 24t \ 60t^2]^T \quad \mathbf{p}_i = [p_{i0} \ p_{i1} \ p_{i2} \ p_{i3} \ p_{i4} \ p_{i5}]^T \quad (13)$$

The sum of jerk $j_i(t)$ is $J(p)$ with optimized coefficients p :

$$J(p) = \sum_{i=1}^m \int_{t_{i-1}}^{t_i} (j_i(t))^2 dt \quad (14)$$

To minimize the sum of jerk $J(p)$ with optimized coefficients p :

$$\min_p \{J(p)\} = \min_p \sum_{i=1}^m \int_{t_{i-1}}^{t_i} (j_i(t))^2 dt, \quad (j_i(t))^2 = (\mathbf{a}^T \mathbf{p}_i)^T (\mathbf{a}^T \mathbf{p}_i) = \mathbf{p}_i^T \mathbf{a} \mathbf{a}^T \mathbf{p}_i \quad (15)$$

We can assume:

$$\mathbf{A}(t) = \mathbf{a} \mathbf{a}^T = \begin{bmatrix} 0 \\ 0 \\ 0 \\ 6 \\ 24t \\ 60t^2 \end{bmatrix} \begin{bmatrix} 0 & 0 & 0 & 6 & 24t & 60t^2 \end{bmatrix} = \begin{bmatrix} 0 & 0 & 0 & 0 & 0 & 0 \\ 0 & 0 & 0 & 0 & 0 & 0 \\ 0 & 0 & 0 & 0 & 0 & 0 \\ 0 & 0 & 0 & 36 & 144t & 360t^2 \\ 0 & 0 & 0 & 144t & 576t^2 & 1440t^3 \\ 0 & 0 & 0 & 360t^2 & 1440t^3 & 3600t^4 \end{bmatrix}$$

And assume:

$$\mathbf{Q}_i = \int_{t_{i-1}}^{t_i} \mathbf{A}(t) dt = \begin{bmatrix} 0 & 0 & 0 & 0 & 0 & 0 \\ 0 & 0 & 0 & 0 & 0 & 0 \\ 0 & 0 & 0 & 0 & 0 & 0 \\ 0 & 0 & 0 & 36t & 72t^2 & 120t^3 \\ 0 & 0 & 0 & 72t^2 & 192t^3 & 360t^4 \\ 0 & 0 & 0 & 120t^3 & 360t^4 & 520t^5 \end{bmatrix}_{t_{i-1}}^{t_i}$$

Therefore, the integral of $j_i(t)^2$ can be elicited as:

$$\int_{t_{i-1}}^{t_i} (j_i(t))^2 dt = \int_{t_{i-1}}^{t_i} \mathbf{p}_i^T \mathbf{A}(t) \mathbf{p}_i dt = \mathbf{p}_i^T \int_{t_{i-1}}^{t_i} \mathbf{A}(t) dt \mathbf{p}_i = \mathbf{p}_i^T \mathbf{Q}_i \mathbf{p}_i \quad (16)$$

So the sum of jerk $J(p)$ can be denoted as:

$$J(p) = \sum_{i=1}^m \int_{t_{i-1}}^{t_i} (j_i(t))^2 dt = \sum_{i=1}^m \mathbf{p}_i^T \mathbf{Q}_i \mathbf{p}_i = [\mathbf{p}_1^T \quad \mathbf{p}_2^T \quad \dots \quad \mathbf{p}_m^T] \begin{bmatrix} \mathbf{Q}_1 & & & \\ & \mathbf{Q}_2 & & \\ & & \ddots & \\ & & & \mathbf{Q}_m \end{bmatrix} \begin{bmatrix} \mathbf{p}_1 \\ \mathbf{p}_2 \\ \vdots \\ \mathbf{p}_m \end{bmatrix} \quad (17)$$

To derive $\min_p J(p)$. The format of $J(p)$ is consistent to a regular Quadratic Programming (QP) function $\min_p \{0.5\mathbf{x}^T Q\mathbf{x} + \mathbf{c}^T \mathbf{x}\}$ and can be subjected to proper constraint equations. Because of the attribution of the QP function, it is a convex function, which means its local minimum is the global minimum. We can apply subsequent steps to solve it with constraints. There are m segments and $6+4(m-1)$ constraints, to impose the initial/final conditions and continuous transitions. After applying Lagrange Multiplier:

$$\left\{ \begin{array}{l} x_1(t_0) = x_1 \\ x_1^{(1)}(t_0) = 0 \\ x_1^{(2)}(t_0) = 0 \\ x_1(t_1) = x_2 \\ x_2(t_1) = x_2 \\ x_1^{(1)}(t_1) = x_2^{(1)}(t_1) \\ x_1^{(2)}(t_1) = x_2^{(2)}(t_1) \\ \vdots \\ x_M(t_M) = x_1 \\ x_M^{(1)}(t_M) = 0 \\ x_M^{(2)}(t_M) = 0 \end{array} \right. \quad \left\{ \begin{array}{l} g_{01} = x_1(t_0) - x_1 \\ g_{02} = x_1^{(1)}(t_0) \\ g_{03} = x_1^{(2)}(t_0) \\ g_{11} = x_1(t_1) - x_2 \\ g_{12} = x_2(t_1) - x_2 \\ g_{13} = x_1^{(1)}(t_1) - x_2^{(1)}(t_1) \\ g_{14} = x_1^{(2)}(t_1) - x_2^{(2)}(t_1) \\ \vdots \\ g_{M1} = x_M(t_M) - x_1 \\ g_{M2} = x_M^{(1)}(t_M) \\ g_{M3} = x_M^{(2)}(t_M) \end{array} \right.$$

We can construct Lagrange functions:

$$L = J(p) + \lambda_{01}g_{01} + \lambda_{02}g_{02} + \lambda_{03}g_{03} + \lambda_{11}g_{11} + \lambda_{12}g_{12} + \lambda_{13}g_{13} + \lambda_{14}g_{14} + \dots + \lambda_{m1}g_{m1} + \lambda_{m2}g_{m2} + \lambda_{m3}g_{m3}$$

And apply partial derivative to elicit sufficient equations to solve polynomial coefficients p_{ij} and multiplier λ_{ij} :

$$\frac{\partial L}{\partial p_{ij}} = 0 \quad \frac{\partial L}{\partial \lambda_{ij}} = 0$$

We can further convert Equations to matrix:

$$\mathbf{A} [p_{10} \quad p_{11} \quad \dots \quad p_{15} \quad p_{20} \quad \dots \quad p_{m5}]^T = \mathbf{b} \quad \mathbf{p} = \mathbf{A}^{-1} \mathbf{b} \quad (18)$$

So far, as long as the time node for each waypoint can be settled down, we can solve the equations by minimizing the jerk. After setting up the scalar function and constraints, we can apply, such as fmincon, to find the optimized time nodes. However, there will be too many iterations, slow and may result in computation crush. An approximate approach can be applied to allocate time nodes. An intuitive minimum jerk trajectory equation for one trajectory moving from location $x = x_i$ to $x = x_f$ in $t = d$ seconds without any redundant segments can be shown as Equation 19:

$$x(t) = x_i + (x_f - x_i)(10(t/d)^3 - 15(t/d)^4 + 6(t/d)^5) \quad (19)$$

However, it cannot be directly applied in our function as it can not guarantee that the trajectory goes through each waypoint. As there are multiple waypoints generated by gradient descent, it is expected that the minimum jerk function can provide timely information and closely follow the gradient trajectory. This is an approximate function, which approximately normalize the distance of position vector $[x_i \ y_i \ z_i]^T$ with i from 0 to m and the approximate entire distance went through would be s_f , and the total distance for each node is denoted as s_n :

$$s_f = \sum_{i=0}^{m-1} \sqrt{(x_{i+1} - x_i)^2 + (y_{i+1} - y_i)^2 + (z_{i+1} - z_i)^2}$$

$$s_n = \sum_{i=0}^{n-1} \sqrt{(x_{i+1} - x_i)^2 + (y_{i+1} - y_i)^2 + (z_{i+1} - z_i)^2}$$

Assuming this is one segmental trajectory regarding distance s_n as the current position w.r.t at the normalized time t_n . initial position 0. We can substitute s_f back into Equation 19:

$$s_n(t_n) = s_f(10(t_n)^3 - 15(t_n)^4 + 6(t_n)^5) \quad (20)$$

There may be two possible solutions while calculating. To solve the time node t_n of each s_n , when $s_n/s_f < 0.5$, $t_n = \min(t_n)$ and when $s_n/s_f > 0.5$, $t_n = \max(t_n)$. This function can approximately allocate optimized time node for each way point, and further apply previous Equation 11-18, can convert spacial trajectory into spatiotemporal trajectory function $x(t)$. And Figure 11 is an example after applying the function in this section compared with iterative optimized function. Temporal trajectory generated by the function in this report can be approximately identical to the optimal result, can compute much faster without iteration and avoid computational crush by complexity.

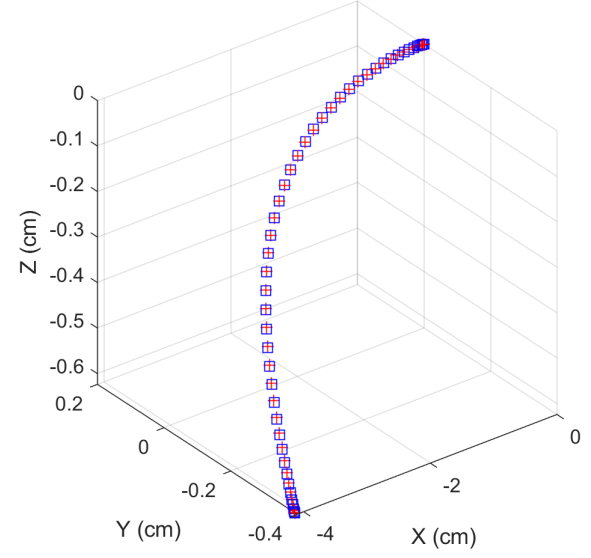


Figure 11: The red cross is the optimal result of the iterative function. The blue square is the result generated by the functions in this report. The sampling period is invariable as 0.05 normalized time. So more sparse represents higher velocity, and more intensive represents the lower velocity.

3.4 Localization and Coordinate System

This section applied two localization approaches for localizing the target position w.r.t. the human body. Pose localization technology named MediaPipe Pose 3D (Lugaresi et al., 2019), working with a depth camera, and the algorithm has been packaged into a repository:

<https://github.com/mingtianand/Upperlimb-Localization>

This program can return the right half body's joints position w.r.t. camera, denoted as cP_s , cP_e and cP_w . Another technology which aims to gather the target's position w.r.t. camera is required. Olson (2011) developed a localization system named AprilTag, which is presented to be better than QR Codes in the localization field in terms of high accuracy and robustness requirements. This report utilized AprilTag technology to localize the targets. The coordinate system for the localization system in this report is presented as Figure 12 schematic. In this coordinate system, assume frame $\{i\}$ is orthogonal to frame $\{0\}$.

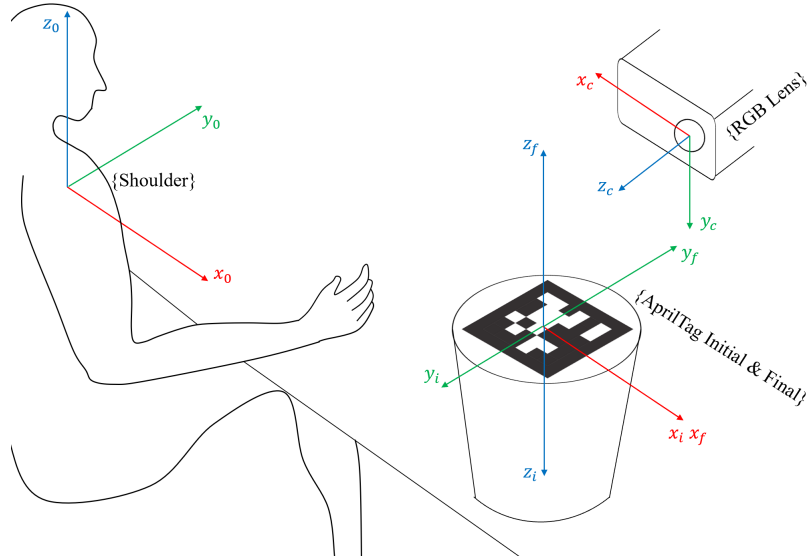


Figure 12: Coordinate system schematic, {Shoulder} reference defined in this report is original reference, {AprilTag Initial} and {RGB LENS} is default reference for AprilTag algorithm. {AprilTag Final} possesses the similar orientation with {Shoulder}, Right x, Forward y and Upward z. Restricting x_0, x_i and x_f always toward right, which can guarantee frame $\{i\}$ and $\{0\}$ are always orthogonal.

Camera intrinsic $[fx, fy, cx, cy]$ is a factory setting, and tag size is defined by using. According to the following code, the transformation matrix from the initial tag to the camera will be gathered with notation as ${}_i^c T$.

```
apriltag.Detector().detect(camera_intrinsic, tag_size)
```

Transformation from camera $\{c\}$ to final tag $\{f\}$ can be calculated as:

$${}_c^f T = \begin{bmatrix} 1 & 0 & 0 & 0 \\ 0 & -1 & 0 & 0 \\ 0 & 0 & -1 & 0 \\ 0 & 0 & 0 & 1 \end{bmatrix} \times {}_i^c T^{-1} \quad (21)$$

And we can transform shoulder, elbow and wrist position into frame $\{f\}$:

$${}^f P_s = {}_c^f T \times {}^c P_s \quad {}^f P_e = {}_c^f T \times {}^c P_e \quad {}^f P_w = {}_c^f T \times {}^c P_w \quad (22)$$

Because frame 0 and f have identical orientation and ${}^0 P_s = [0 \ 0 \ 0 \ 1]^T$:

$${}^0 P_f = -{}^f P_s \quad {}^0 P_e = {}^f P_e - {}^f P_s \quad {}^0 P_w = {}^f P_w - {}^f P_s \quad (23)$$

From Equations 21-23, the shoulder, elbow, wrist and target position w.r.t. frame $\{0\}$ are gathered. As the target is a cup, the real center of the cup is not the center of the tag, so neglect the irregular shape of the cup and impose a compensation by the height of the target denoted as h_t :

$${}^0 P_f = [{}^0 P_{fx} \ {}^0 P_{fy} \ {}^0 P_{fz} - 0.5h_t]^T \quad (24)$$

3.5 Simulation

So far, sufficient technologies have been selected or hypothesized. By gradient descent and minimum jerk, a spatiotemporal trajectory can be generated, and there are no redundancy relative problems pending because forward kinematics instead of inverse kinematics will be applied for trajectory generation. From Table 3, four possible solutions after adding time information are simulated shown as Figure 13.

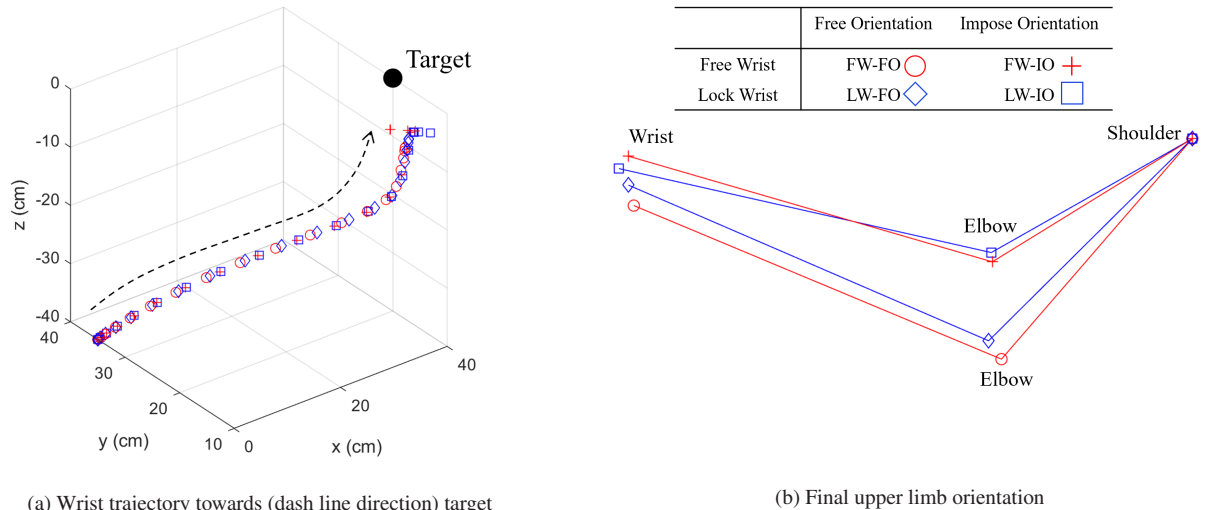


Figure 13: Diagram of simulation results of four models FW-FO, FW-IO, LW-FO and LW-IO.

From Figure 13a, four models do not present apparent differences while in the initial stage but will demonstrate differences in the final stage. From Figure 13b, four models have a different final states to finish the reaching movement. Imposing orientation or not has a more noticeable impact on the result, but whether locking the wrist does not significantly impact the results. This report concerns wrist trajectory and final forearm orientation. All these four models can work well in simulation but reveal four different results. A proper experiment is necessary to be conducted. The experiment data is expected to tell which model is closer to the natural human-like movement or which model has lower errors on wrist trajectory and final forearm orientation.

4 Experiment

4.1 Experiment Protocol

4.1.1 Objective

To quantify how healthy people generally reach target objects in different locations for drinking and evaluate a related reaching model.

4.1.2 Subjects

5 healthy human beings who is not familiar with this project.

4.1.3 Equipment and Setup

Chair, table with adjustable height, weighted regular coffee cup, localization device, and a splint to lock the wrist rotations. The initial status for each subject to reach the cup is defined in Figure 14. Figure 14a manifest two initial gestures for each subject without locking the subject's wrist. And 14a is two identical postures whose wrist will be locked using a splint. Locking or freeing the wrist will be respectively relative to models. Therefore there will be four groups of data for each subject.

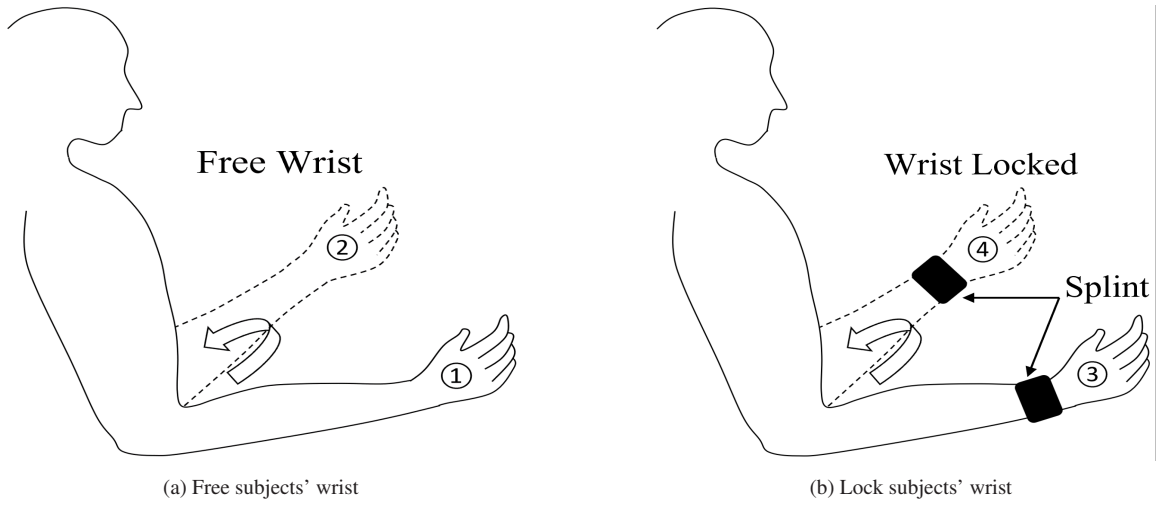


Figure 14: Initial status for each subject

For normalizing the targets' position and neglect the uncertainty about particular position. Multiple cups will be set up based on the subject's upper limb length, horizontal and vertical 30° shown as Figure 15.

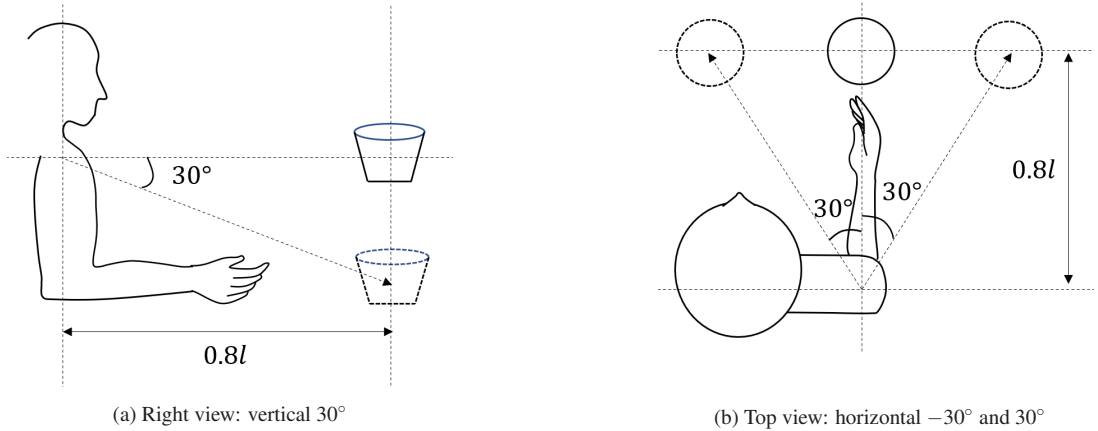


Figure 15: Schematic about normalizing the target positions based on each subject's upper limb length l .

There will be six targets in total, and below is the practical experiment set up and the schematic of six targets on a vertical platform, shown as Figure 16.

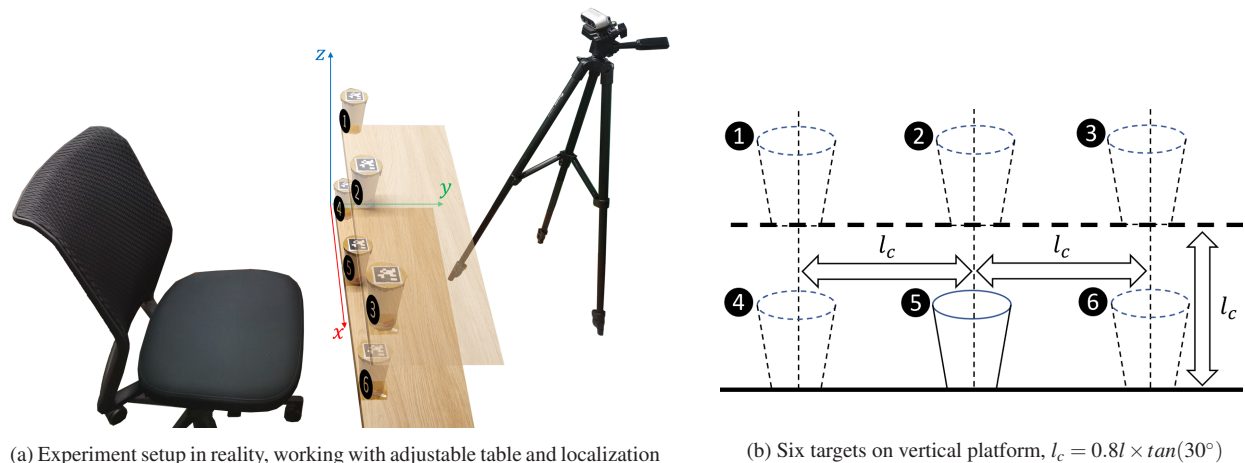


Figure 16: Experiment setup and its schematic

4.1.4 Routine

1. Initial posture 1
2. Set up experimental environment
3. Initialize the localization system
4. Randomly select the position 1-6 to place the cup
5. Ask the subject to reach the cup for drinking
6. Repeat step 5 three times
7. Break and repeat steps 4-7
8. Fix the wrist and repeat step 1-7
9. Initial posture 2 and repeat steps 2-8

4.1.5 Measurements

Before setting up experiment environment, Subject ID will be recorded and measure subject's upper arm length (UL), fore arm length (FL) and palm length (PM). While in experiment, will collect data incorporating time t . shoulder, elbow, wrist position w.r.t camera cP_s , cP_e , cP_w and transformation matrix from initial tag to camera ${}_i^cT$ in each camera frame. The data set expected to be collected is listed up in Table 4. We can apply previous Equation 21-24 to calculate ${}^0P_s = \mathbf{0}$, 0P_e , 0P_w and 0P_f .

Subject ID	UL (cm)	FL (cm)	PL (cm)	t (ms)	cP_s (cm)	cP_e (cm)	cP_w (cm)	${}_i^cT$
------------	---------	---------	---------	----------	----------------	----------------	----------------	-----------

Table 4: Data expected to be collected for each subject

4.1.6 Expected Outcome

The expected outcome is that the following errors are acceptable.

1. Final forearm orientation related to target error w.r.t. model.

$${}^0r_{ew}^{exp} = {}^0P_w^{exp} - {}^0P_e^{exp} \quad {}^0r_{ew}^{mod} = {}^0P_w^{mod} - {}^0P_e^{mod}$$

$$E = \arccos\left(\frac{{}^0r_{ew}^{exp} \cdot {}^0r_{ew}^{mod}}{|{}^0r_{ew}^{exp}| |{}^0r_{ew}^{mod}|}\right)$$

2. Wrist, which is controlled by the robot, the positional trajectory error w.r.t. model.

$$E = \sqrt{({}^0P_{wx}^{exp} - {}^0P_{wx}^{mod})^2 + ({}^0P_{wy}^{exp} - {}^0P_{wy}^{mod})^2 + ({}^0P_{wz}^{exp} - {}^0P_{wz}^{mod})^2}$$

3. If the former errors are not acceptable, we will calculate the average error on each joint angle during the trajectory w.r.t. model to define the reason.

$$E_i = \frac{1}{N} \sum_{j=1}^N (|q_i^{exp}(t_j) - q_i^{mod}(t_j)|)$$

4.2 Experiment Results and Analysis

Experiments on five subjects have been conducted. Every subject was asked to reach one target three times, and the variance for these three reaching movements for each target for each subject is integrated as Figure 17. It is expected that the model's error relative to the experiment is lower or not much more significant than this variance, representing that the model's uncertainty for a particular subject is acceptable because the subject can present uncertainty for each movement. It should be noticed that the repeated movements with more possibilities to be similar. So the derived variance in Figure 17 is a lower-variance condition. The average variance of wrist trajectory is about 3cm and the maximum variance except outlier is about 7cm from Figure 17a. From Figure 17b, the average variance of final forearm orientation is very small, the maximum variance except outlier is about 10°. Such a small average variance imply that the localization system is stable.

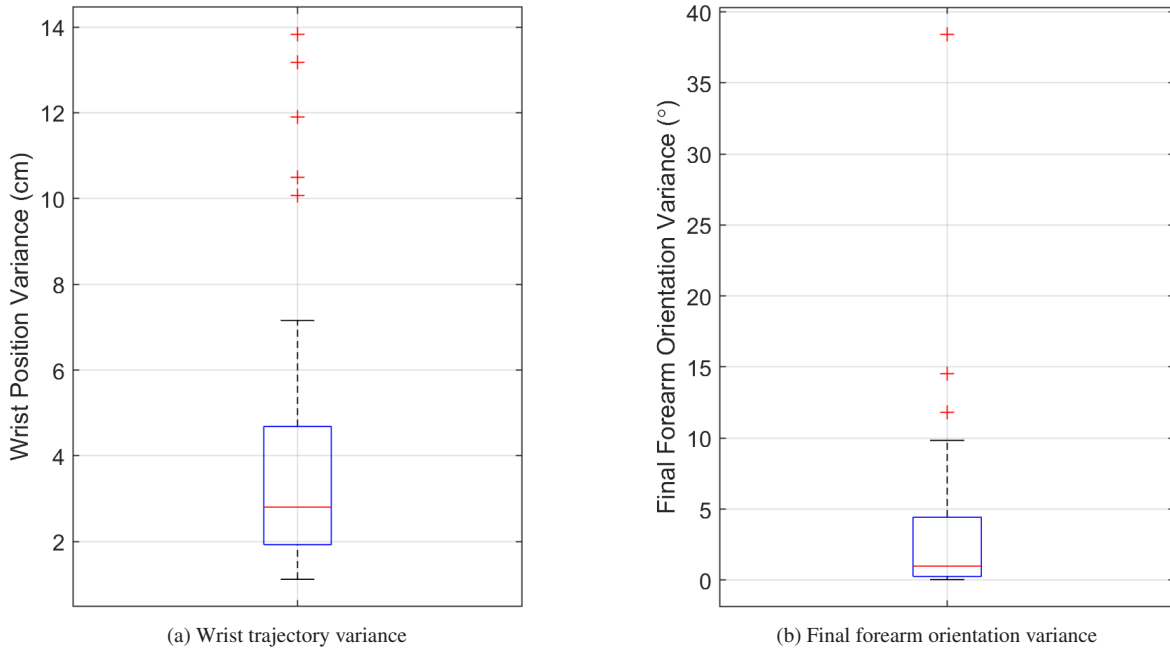


Figure 17: The variance of each three times' repeated movements

Set the model according to the subjects' upper limb length. And initialize the model's initial posture according to posture derived from each experiment data set to neglect the uncertainty from the initial condition. In this model, the cost function error of gradient descent ε is 2cm , the step size λ is 0.002 and weight to impose orientation α is 10. Whether free the wrist in the model will be relative to whether the data set is gathered while freeing the wrist. Besides, the model will free and impose orientation for each data set. Therefore, the final amount of error data is equal to twice over experiment data. And the final error of wrist trajectory and final forearm orientation is demonstrated in Figure 18.

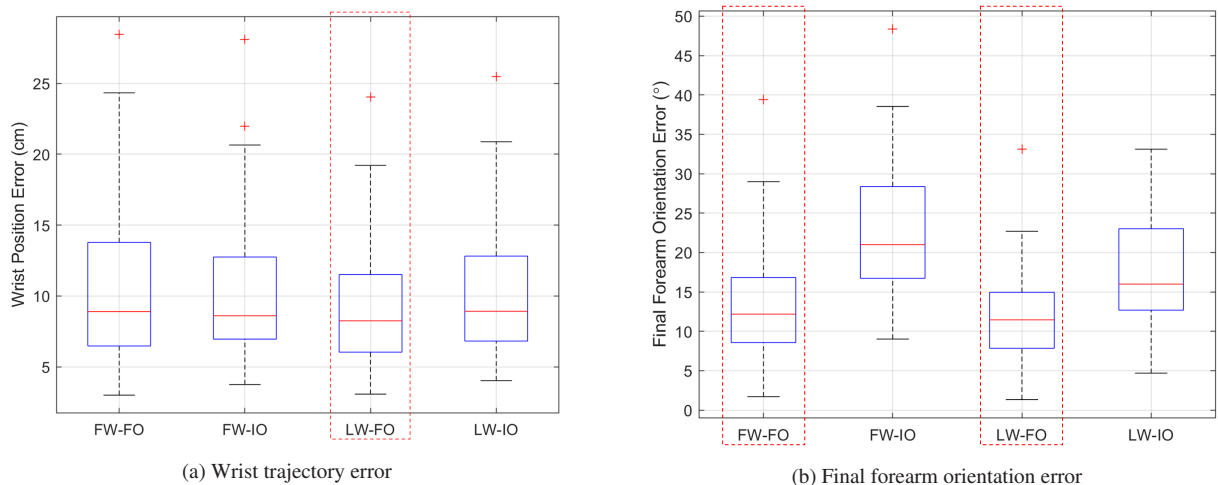


Figure 18: Error for four models: FW-FO: Free Wrist-Free Orientation. FW-IO: Free Wrist-Impose Orientation. LW-FO: Lock Wrist-Free Orientation. LW-IO: Lock Wrist-Impose Orientation.

From Figure 18a, the wrist trajectory error does not present a significant difference, with all average errors being lower than 10cm . LW-FO model has the lowest average error but can not be explained as definitely better. As for the final forearm orientation error shown as Figure 18b, the difference is significant, which reveals that the FO model, including FW-FO and LW-FO, is much better than the IO model, with an average error of around 12° . Therefore, the FO model is more representative relative to the IO mode. Considering the FO model, there is a possibility that different initial postures may impact the result. So the further comparison between initial posture 1 (IP1) and initial posture 2 (IP2) is demonstrated in Figure 19.

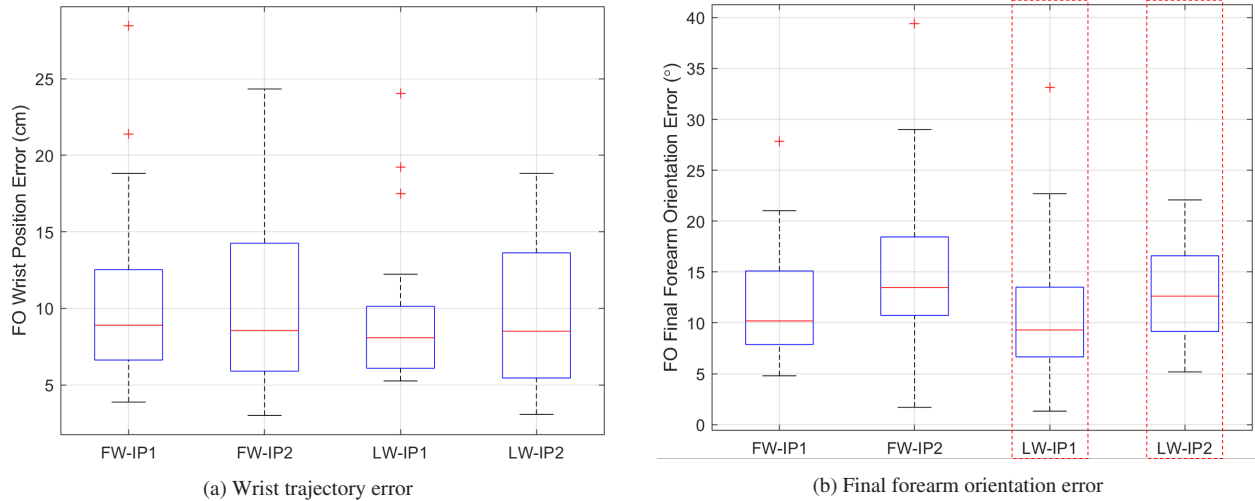


Figure 19: Error for FO models under different Initial posture IP: FW-IP1: Free Wrist-Initial Posture 1. FW-IP2: Free Wrist-Initial Posture 2. LW-IP1: Lock Wrist-Initial Posture 1. LW-IP2: Lock Wrist-Initial Posture 2.

From Figure 19a, same as the analysis before, no significant difference on average value, which means initial posture does not significantly impact the wrist trajectory. The large variance of IP2 may be relevant to localization accuracy. But for final forearm orientation shown as 19b. IP2 may result in a larger error, but no greater than 5° . This result can be explained by one example condition shown in Figure 20.

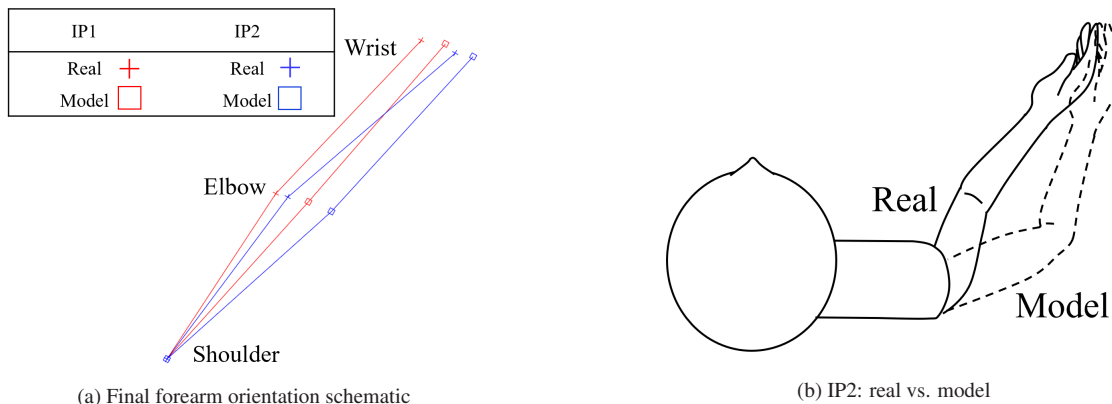


Figure 20: One example indicates the difference between real vs. model among initial posture 1 (IP1) and initial posture 2 (IP2).

From Figure 20a, IP2 real and model have a more significant orientational difference. And the schematic of this condition has been depicted in Figure 20b. While in IP2, a human may externally rotate the shoulder to reach the target, but the model will internally rotate the shoulder. However, this is a particular condition that does not possess universality. In summary, even though IP2 has a more significant error for forearm orientation. It is not sufficient to criticize that this model is not acceptable for IP2. Merely IP1 is more representative of this model. As an additional part of this project, it will be interesting to impose Equation 8 to make the joint angle variable while generating trajectory. The Equation 8 enforces shoulder elevation, which may make the upper arm contribute less than the forearm. In this example, the step size is 0.5λ while rising arm and 1.5λ while descending arm. And the result is shown in Figure 21.

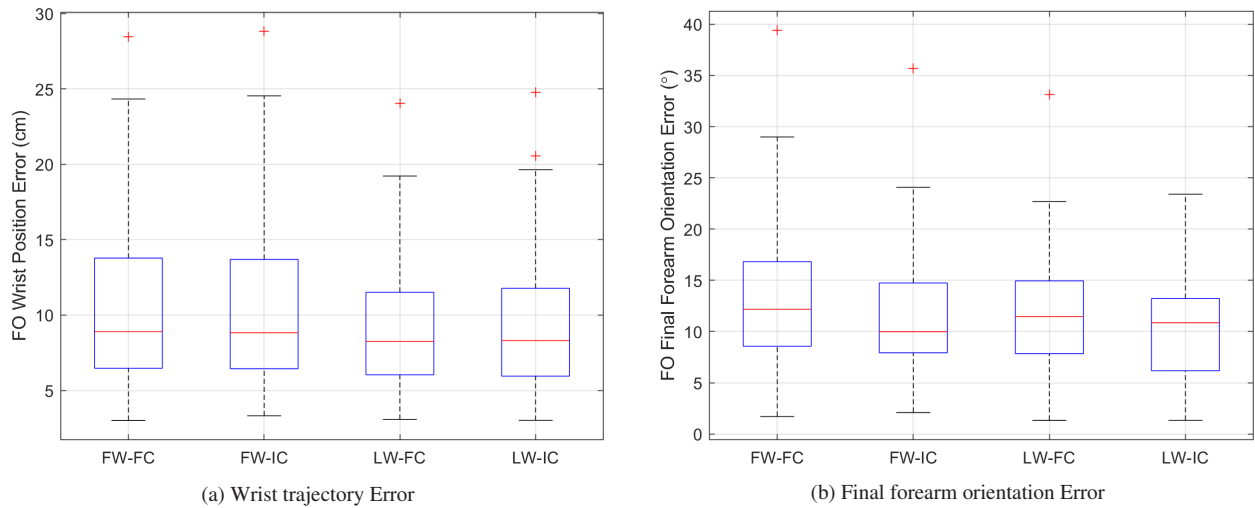


Figure 21: Error for FO models free or imposing constraint Equation 8: FW-FC: Free Wrist-Free Constraint. FW-IC: Free Wrist-Impose Constraint. LW-FC: Lock Wrist-Free Constraint. LW-IC: Lock Wrist-Impose Constraint.

From Figure 21a, there is still no significant difference. Nevertheless, a preliminary result can be illustrated from Figure 21b that Equation 8 may be feasible for some groups because the average error is slightly lower. But considering its complexity, the delivery of this report will not apply this function.

5 Conclusion

A set of ADLs is necessary for rehabilitation, and rehabilitation robotics such as EMU is missing the function of automatical control to help severe patients. Based on the destination is to help more people walking out from the suffering of stroke. This report intends to implement automatical and dynamical control of ADL reaching movement. An innovative method to generate spatiotemporal trajectory is presented in this report by integrating gradient descent and minimum jerk. Localization technologies MediaPipe Pose 3D and AprilTag are applied to the experiment. From the simulation result, our method is feasible because it can realize dynamical reaching movement after solving problems about redundancy and the absence of time. Experiment results reveal that the free orientation model is more representative, with wrist trajectory error lower than 10cm. The final forearm orientation error is around 12° and has the potential to be further investigated because its final forearm orientation error can reach below 10° after imposing a variable step-size function.

Because the EMU robotic is operated by locking the users' wrist, this report also researched a lot to eliminate the possibility that locking or freeing the wrist is typical. And the experiment results verify that this is not a significant impact that is supposed to be concerned. Our model can both be applied for wrist-locked robotic or wrist-free robotic.

The concluded model error is still more significant than the average human repeated reaching movement variance. This is reasonable because repeated movement is supposed to possess lower variance. So if taking the maximum variance except for outliers as the criteria, the model's errors are acceptable for a general reaching movement.

6 Discussion and Recommendation

In this report, trunk contribution is assumed to be neglected, but it can not be neglected in reality, so our model can be extended by trunk DoF to be further evaluated. And this report entirely applies normalized time, so if needed, a general duration can be defined by more subjects. Furthermore, hand orientation has been illustrated to be sensitive to target features, which means the evaluation of this model may not be available for reaching other kinds of a target, such as reaching a spoon. Because this model is evaluated by a healthy group, and the difference in reaching movement between stroke patients and healthy human beings is sensitive to the stroke's

degree of severity. So the effectiveness after imposing this general training by automatical control may be variable for different groups and require further research.

The amount and age of subjects in the experiment are relatively limited, so optimizing this model requires more subjects. A possible optimization approach includes making the step size variable. The errors of the localization system applied in this report are neglected. Regarding the error of the localization algorithm and physical depth camera, even though the error of this model may be larger than the conclusion, the model has sufficient functions to realize control, merely not so human-like. Therefore, collecting data from more subjects and applying a more accurate localization system for further study is recommended. Because this report only evaluates the reaching movement, our model can be evaluated by more ADLs such as drinking movement. The basic idea in this report may be developed for other applications, such as rehabilitation for lower limbs, and may be extended into other fields, such as path programming for bionic robotics.

While applying the model in this report, it is recommended to properly set the parameters, such as gradient descent step size. There are methods, such as backtracking, that can set parameters automatically. After tuning the parameters manually or automatically, the model may be improved to be more human-like.

References

- Alt Murphy, M., Willén, C., & Sunnerhagen, K. S. (2012). Movement kinematics during a drinking task are associated with the activity capacity level after stroke. *Neurorehabilitation and neural repair*, 26(9), 1106–1115.
- Choi, W., Won, J., Lee, J., & Park, J. (2017). Low stiffness design and hysteresis compensation torque control of sea for active exercise rehabilitation robots. *Autonomous robots*, 41(5), 1221–1242.
- Collins, K. C., Kennedy, N. C., Clark, A., & Pomeroy, V. M. (2018). Getting a kinematic handle on reach-to-grasp: A meta-analysis. *Physiotherapy*, 104(2), 153–166.
- Costa e Silva, E., Costa, F., Bicho, E., & Erlhagen, W. (2011). Nonlinear optimization for human-like movements of a high degree of freedom robotics arm-hand system. *International Conference on Computational Science and its Applications*, 327–342.
- Flash, T., & Hogan, N. (1985). The coordination of arm movements: An experimentally confirmed mathematical model. *Journal of neuroscience*, 5(7), 1688–1703.
- Fong, J., Crocher, V., Tan, Y., Oetomo, D., & Mareels, I. (2017). Emu: A transparent 3d robotic manipulandum for upper-limb rehabilitation. *2017 International Conference on Rehabilitation Robotics (ICORR)*, 771–776.
- García Álvarez, A., Roby-Brami, A., Robertson, J., & Roche, N. (2017). Functional classification of grasp strategies used by hemiplegic patients. *PLoS One*, 12(11), e0187608.
- Gentilucci, M., Daprati, E., Gangitano, M., & Saetti, M. C. (1996). On orienting the hand to reach and grasp an object. *Neuroreport: An International Journal for the Rapid Communication of Research in Neuroscience*.
- Gulletta, G., Erlhagen, W., & Bicho, E. (2020). Human-like arm motion generation: A review. *Robotics*, 9(4), 102.
- Hoff, B., & Arbib, M. A. (1993). Models of trajectory formation and temporal interaction of reach and grasp. *Journal of motor behavior*, 25(3), 175–192.
- Lugaresi, C., Tang, J., Nash, H., McClanahan, C., Uboweja, E., Hays, M., Zhang, F., Chang, C.-L., Yong, M. G., Lee, J., et al. (2019). Mediapipe: A framework for building perception pipelines. *arXiv preprint arXiv:1906.08172*.
- Mehrholz, J., Pollock, A., Pohl, M., Kugler, J., & Elsner, B. (2020). Systematic review with network meta-analysis of randomized controlled trials of robotic-assisted arm training for improving activities of daily living and upper limb function after stroke. *Journal of neuroengineering and rehabilitation*, 17(1), 1–14.
- Murphy, M. A., Willén, C., & Sunnerhagen, K. S. (2011). Kinematic variables quantifying upper-extremity performance after stroke during reaching and drinking from a glass. *Neurorehabilitation and neural repair*, 25(1), 71–80.
- Nakayama, H., Jørgensen, H. S., Raaschou, H. O., & Olsen, T. S. (1994). Recovery of upper extremity function in stroke patients: The copenhagen stroke study. *Archives of physical medicine and rehabilitation*, 75(4), 394–398.
- Nam, H. S., Hong, N., Cho, M., Lee, C., Seo, H. G., & Kim, S. (2019). Vision-assisted interactive human-in-the-loop distal upper limb rehabilitation robot and its clinical usability test. *Applied Sciences*, 9(15), 3106.
- Nichols-Larsen, D. S., Clark, P., Zeringue, A., Greenspan, A., & Blanton, S. (2005). Factors influencing stroke survivors' quality of life during subacute recovery. *Stroke*, 36(7), 1480–1484.
- Olson, E. (2011). Apriltag: A robust and flexible visual fiducial system. *2011 IEEE international conference on robotics and automation*, 3400–3407.
- Parker, V., Wade, D., & Hewer, R. L. (1986). Loss of arm function after stroke: Measurement, frequency, and recovery. *International rehabilitation medicine*, 8(2), 69–73.
- Popovic, M. R., Popovic, D. B., & Keller, T. (2002). Neuroprostheses for grasping. *Neurological research*, 24(5), 443–452.
- Riener, R., Lunenburger, L., Jezernik, S., Anderschitz, M., Colombo, G., & Dietz, V. (2005). Patient-cooperative strategies for robot-aided treadmill training: First experimental results. *IEEE transactions on neural systems and rehabilitation engineering*, 13(3), 380–394.

- Rounis, E., Zhang, Z., Pizzamiglio, G., Duta, M., & Humphreys, G. (2017). Factors influencing planning of a familiar grasp to an object: What it is to pick a cup. *Experimental Brain Research*, 235(4), 1281–1296.
- Schaefer, S. Y., DeJong, S. L., Cherry, K. M., & Lang, C. E. (2012). Grip type and task goal modify reach-to-grasp performance in post-stroke hemiparesis. *Motor control*, 16(2), 245–264.
- Schambra, H. M., Parnandi, A., Pandit, N. G., Uddin, J., Wirtanen, A., & Nilsen, D. M. (2019). A taxonomy of functional upper extremity motion. *Frontiers in neurology*, 857.
- Torres, E. B., & Zipser, D. (2002). Reaching to grasp with a multi-jointed arm. i. computational model. *Journal of neurophysiology*, 88(5), 2355–2367.
- Wisneski, K. J., & Johnson, M. J. (2007). Quantifying kinematics of purposeful movements to real, imagined, or absent functional objects: Implications for modelling trajectories for robot-assisted adl tasks. *Journal of NeuroEngineering and Rehabilitation*, 4(1), 1–14.
- Witkin, A., Fleischer, K., & Barr, A. (1987). Energy constraints on parameterized models. *Proceedings of the 14th annual conference on Computer graphics and interactive techniques*, 225–232.
- Wu, C.-y., Trombly, C. A., Lin, K.-c., & Tickle-Degnen, L. (2000). A kinematic study of contextual effects on reaching performance in persons with and without stroke: Influences of object availability. *Archives of physical medicine and rehabilitation*, 81(1), 95–101.